Geophys. J. Int. (1998) **135,** 876–892

The M_L 5.3 Epagny (French Alps) earthquake of 1996 July 15: a long-awaited event on the Vuache Fault

François Thouvenot,[1] Julien Frechet,[1] Paul Tapponnier,[2] Jean-Charles Thomas,[1] Benoıt Le Brun,[1] Gilles Menard,[3] Robin Lacassin,[2] Liliane Jenatton,[1] Jean-Robert Grasso,[1] Olivier Coutant,[1] Anne Paul[1] and Denis Hatzfeld[1]

[1] Laboratoire de Geophysique Interne et de Tectonophysique, Observatoire de Grenoble (CNRS/UJF), Boıte Postale 53, 38041 Grenoble cedex 9, France. E-mail: thouve@ujf-grenoble.fr

[2] Laboratoire de Tectonique et de Mecanique de la Lithosphere, Institut de Physique du Globe, Case 89, 75252 Paris cedex 05, France

[3] Laboratoire de Geodynamique des Chaines Alpines, Campus Scientifique, Savoie Technolac, 73376 Le Bourget du Lac cedex, France

Accepted 1998 June 25. Received 1998 June 22; in original form 1997 October 6

SUMMARY

The M_L 5.3 Epagny earthquake that occurred on 1996 July 15 in the vicinity of Annecy (French Alps) was the strongest event to shake southeastern France in the last 34 years. Moderate to serious damage in the Annecy area is consistent with MSK intensities of VII–VIII. This earthquake occurred on the Vuache Fault, a geologically well-known, morphologically clear, NW–SE-trending strike-slip fault that links the southern Jura Mountains with the northern Subalpine chains. The hypocentre was located in Mesozoic limestones at shallow depths (1–3 km). The focal mechanism indicates left-lateral strike-slip motion on a N136°E-striking plane dipping 70° to the NE. Abundant field evidence was gathered in the days following the main shock. Several hundred aftershocks were recorded thanks to the rapid installation of a 16-station seismic network. All aftershocks occurred along the southernmost segment of the Vuache Fault, defining a 5-km-long, 3.5-km-deep, N130°E-striking rupture zone dipping 73° to the NE. The fault plane solutions of 60 aftershocks were found to be consistent with left-lateral slip on NW–SE-striking planes. At the SE tip of the aftershock zone we found ground cracks parallel to the fault close to the Annecy–Meythet airport runway; at the NW tip, near Bromines, we observed left-lateral displacement of concrete walls in a building. We also noticed flow changes in two springs close to that locality. Geodetic levelling across the fault revealed about 1 cm of uplift for the region north of the fault. The recording of aftershocks with a six-station accelerometric network showed that lacustrine deposits locally amplified the ground motion up to eight times, which explains how this moderate-magnitude shock could cause such heavy damage. Historical records draw attention to the central segment of the Vuache Fault, which has been locked for at least 200 years. Situated NW of the 1996 aftershock zone, between the Mandallaz and Vuache mountains, this segment forms a 12-km-long potential seismic gap where other M5 events or one single M6 event might occur.

Key words: Alps, Annecy, fault tectonics, seismicity, seismic quiescence.

INTRODUCTION

The seismicity of southeastern France and of the nearby western Alps is moderate: although events with magnitudes usually lower than 1.5 are observed daily, only a few events with magnitude higher than 3 occur each year. Most epicentres are located close to the French–Italian border (e.g. Thouvenot 1996), where two particularly active seismic belts have long been recognized, one along the Penninic Frontal Thrust (the major tectonic boundary between the external and internal Alps, see Fig. 1) and the other along the western edge of the Po Plain. In contrast, in the external Alps, and especially in the Savoie and Dauphine regions (the Annecy–Chambery and Grenoble areas, respectively), seismicity is more diffuse. The

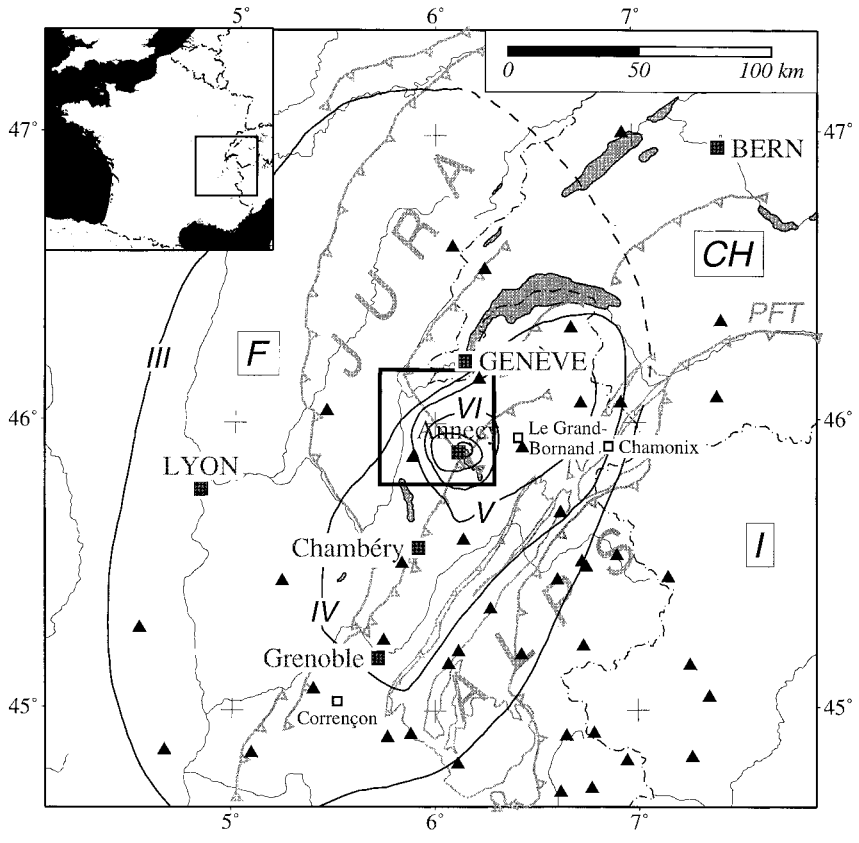

Figure 1. Area shaken by the 1996 July 15 Epagny earthquake. Isoseismal curves from the Bureau Central Seismologique Français. Triangles show permanent seismic stations. Chamonix, Corrençon and Le-Grand-Bornand are the sites of three damaging earthquakes discussed in the text. Principal Late Cenozoic thrusts are indicated. PFT = Penninic Frontal Thrust. Boxes show frames of Figs 2(b) and 3. Inset shows geographical location.

rare earthquakes that occur in these regions often have magnitudes greater than 2 and are frequently felt. Although long underestimated, the number of felt events in southeastern France probably amounts to several tens per year.

In the northern French Alps, since the turn of the century, Rothe (1941, 1972), Vogt (1979) and Lambert & Levret-Albaret (1996) have reported only five earthquakes that have reached a maximum intensity of VII on the MSK (Medvedev–Sponheuer–Karnik) intensity scale. Only two of these reached damaging intensities of VII–VIII (Fig. 1), the first on 1905 April 29 at Chamonix, 60 km east of Annecy (estimated magnitude: 5.7), and the second on 1962 April 25 at Corrençon, 25 km SW of Grenoble ($M_L = 5.3$). The last earthquake to cause minor damage in the region (Frechet et al. 1996) occurred at Le Grand-Bornand on 1994 December 14 ($M_L = 5.1$, $I_0 =$ VI–VII), and was felt in Annecy (I = V), 25 km to the west.

The M_L 5.3 earthquake that struck the Annecy area on 1996 July 14 was therefore the highest-magnitude event in southeastern France since the Corrençon earthquake, which occurred 34 years previously. It is also exceptional in its proximity, in both time and space, to the 1994 Le Grand-Bornand earthquake. It caused significant damage in the city for the first time in about 150 years (see 'Previous seismic activity' below). However, the relationship between the two events is unclear. The 10-km-deep Le Grand-Bornand hypocentre was located within the basement of the Subalpine chains, on a hidden, hitherto unknown fault, with no clear connection with surface tectonics. The Annecy hypocentre was shallow and was located very close to the trace of the Vuache Fault, a major, long-identified geological and morphological cut across the shallow crustal features of the region (Fig. 2).

Regions of moderate seismicity such as southeastern France are often places where the risk is increased by industrial development. They are characterized by the occurrence, once or twice a century, of earthquakes with magnitudes larger than 6 that strike at different places in the region. For a given place, on a given fault, the recurrence time can straddle centuries or even millennia. Very low slip rates make the identification of active faults difficult because clues indicating weak deformation are rarely observed in Quaternary sediments. To understand the relations between surface tectonics and seismicity better, it is therefore of cardinal importance—whenever and wherever the opportunity arises—to study both the detailed geometry of seismogenic faults and the rupture propagation of earthquakes.

REGIONAL TECTONICS AND SEISMICITY OF THE ANNECY AREA

Tectonic setting

Crustal thickening in the northern Subalpine chains and the Jura Mountains (Fig. 1) is a direct result of the ongoing convergence between the European and Adriatic plates. The corresponding shortening is accommodated by Plio-Quaternary thrust faults, and by motion along oblique

(a)

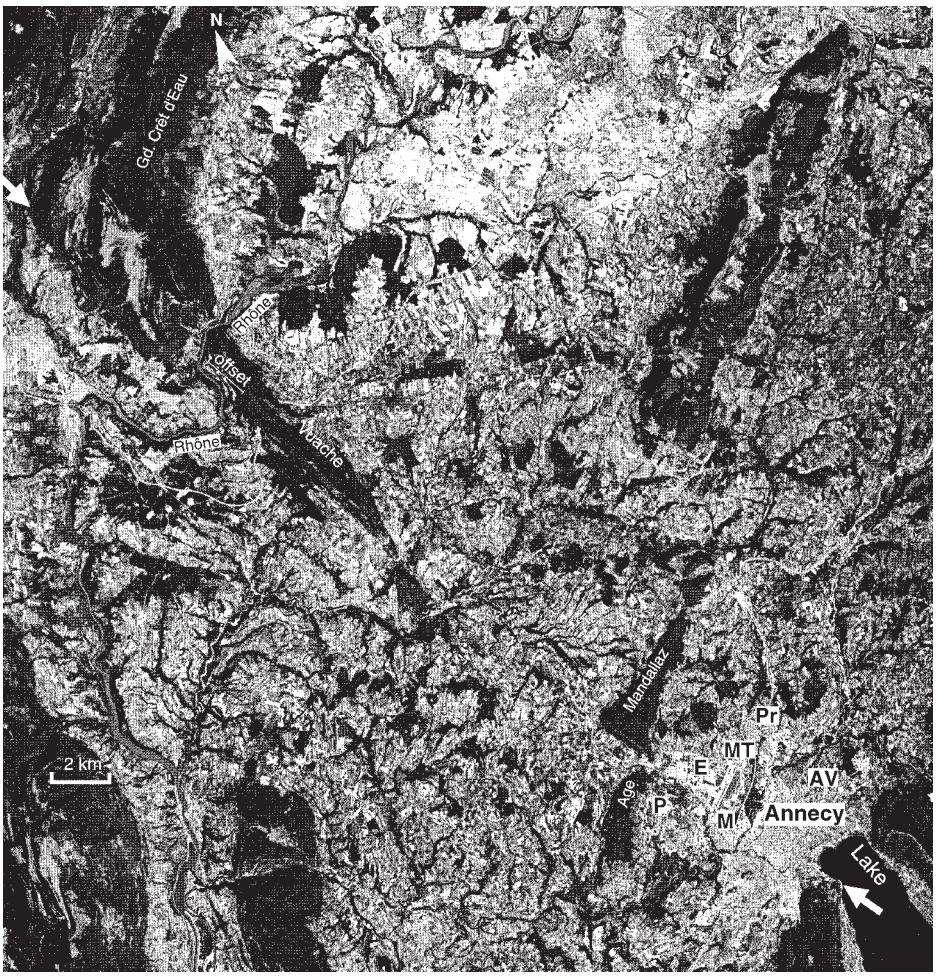
N
Gd Crêt d'Eau
Rhône
Offset
Vuache
Rhône
Mandallaz
Pr
MT
E
AV
P
M
Annecy
Âge
Lake
2 km

(b)

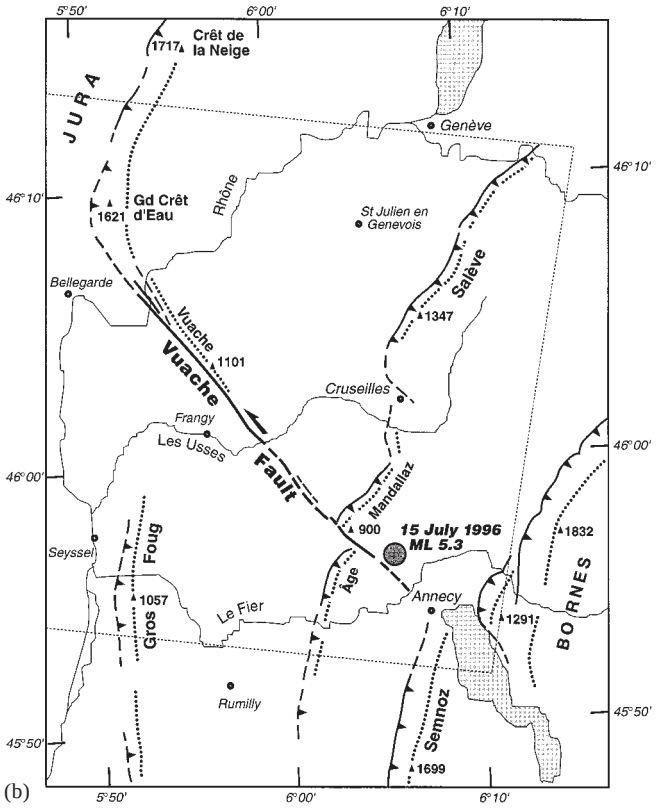
5°50′
6°00′
6°10′
Crêt de la Neige
1717
JURA
Genève
46°10′
Gd Crêt d'Eau
1621
Rhône
St Julien en Genevois
Salève
1347
Bellegarde
Vuache
1101
Vuache Fault
Cruseilles
Frangy
Les Usses
46°00′
Mandallaz
900
15 July 1996
ML 5.3
1832
Seyssel
Foug
Gros
1057
Le Fier
Âge
Annecy
1291
BORNES
Rumilly
Semnoz
1699
45°50′

(b)

(c)

Figure 2. (a) Panchromatic Spot image (K-J/49-257, 1990-08-19) of the Vuache Fault (shown with arrows) between Lake Annecy (lower right corner) and Grand Cret d'Eau (upper left corner). E = Epagny (epicentre), MT = Metz-Tessy, M = Meythet, P = Poisy and Pr = Pringy denote NW suburbs of Annecy where most damage in the 1996 Epagny earthquake occurred; AV = Annecy-le-Vieux suffered less damage. (b) Structural framework and main recent faults of the area shown in (a) (dotted box). West-verging thrusts (dashed where hidden) underlie anticlines in the Mesozoic cover (dotted). The Vuache Fault joins Semnoz and Grand Cret d'Eau. (c) Airborne view of the Vuache mountain as seen from the SSW. The Vuache Fault trace is clearest at the southern foot of the mountain, roughly along the limit between forest and cultivated fields. Jura mountains in background.

strike-slip faults. In the southern Jura Mountains, many N140°E–N150°E-striking, left-lateral strike-slip faults cut and offset the more common NNE-trending anticlines and synclines. The Vuache Fault is one of the most prominent of these faults. First described by Schardt (1891) in the Bellegarde area, this 30-km-long fault connects the southern Jura Mountains to the northern Subalpine chains across the Geneva–Rumilly molasse basin (Figs 2a and b).

The fault trace is especially clear both to the SE, along the SW flank of the Mandallaz Mountain, NW of Annecy, and to the NW, along the SW flank of the Vuache Mountain (Fig. 2c). Near the canyon dug into this mountain by the Rhone river (Figs 2a and b), the fault appears to split into several branches (Arikan 1964). The southernmost branch then appears to veer along the western flank of the Grand Cret d'Eau, where it becomes a thrust. This geometry suggests that the Vuache Fault is a lateral thrust ramp that accommodates differential shortening between the Jura and the northern Subalpine chains. The continuation of the fault into the Jura Mountains remains unclear (Chauve et al. 1980).

In its middle stretch, between the Vuache and Mandallaz mountains, across the Miocene molasse basin, the fault is difficult to trace at the surface. Only faint aligned morphological discontinuities in stream channels and hillsides are visible. We attribute this decrease in morphological expression to extensive reshaping of the surface geology under glacial and periglacial conditions during and after the last glacial maximum.

The Vuache Fault has been considered to be a reactivated Variscan structure, reactivated particularly during the Alpine orogeny (Charollais et al. 1983), but it remains unclear how much of the basement was involved in this process. According to Blondel et al. (1988), the fault was reactivated during the Cretaceous and accommodated at least four tectonic phases during the Cenozoic. Blondel et al. related left-lateral motion on the fault to the last tectonic phase, which began in the Upper Miocene.

The finite horizontal displacement along the fault is not precisely known owing to a lack of unambiguous geological markers. Estimates range between 1 and 15 km (Charollais et al. 1983), which implies a very wide range of slip rates, from 0.08 to 3 mm yr^{-1}, if averaged over the last 5–12 Myr. The offset possibly varies along strike (Rigassi 1977). However, one key geomorphological marker of Plio-Quaternary movement on the fault may be the left-lateral offset of the Rhone River valley. It amounts to 1–3 km, and it must reflect motion on the fault since the river course became locked, by incision, into the limestones of the Vuache–Cret d'Eau mountain (Figs 2a and b). This amount would represent, as elsewhere along major active faults (e.g. Gaudemer et al. 1995), a lower bound for the finite offset of the Vuache Fault.

Previous seismic activity

An earthquake with intensity VII (MSK), apparently similar in its effects to the 1996 event, occurred on 1839 August 11 in the Annecy area (Fig. 3). It is considered the strongest shock of a sequence of at least seven shocks felt between August 7 and 27 (Billiet 1851; Serand 1909). Another strong shock occurred on August 16. These two shocks caused the collapse of many chimneys in the city of Annecy. According to the Journal de Geneve (1839), a 10-year-old child was killed on August 16 following one such collapse. Although no mention is made in the Journal de Geneve (1839)—which shows how biased press reports can be, even in those days—the August 11 shock was felt 30 km to the north in Geneva, where glasses fell off tables in elevated buildings (Correspondenzblatt 1840). It was faintly felt 40 km to the SW in Chambery, the main town and administrative centre of Savoie at the time. However, it was not reported in villages closer to Annecy (Journal de Savoie 1839; Correspondenzblatt 1840). This might indicate a shallow focus in the Annecy Basin. The August 16 shock was only faintly felt in Geneva (Correspondenzblatt 1840).

The 1936 April 17 'Frangy' event is the first well-recorded earthquake that can be unambiguously ascribed to slip on the Vuache Fault. It occurred at the SE end of the Vuache Mountain, 20 km NW of Annecy. Moderate damage (MSK VII) was caused in a limited area, but there are no felt reports from Annecy, which suggested to Rothe (1941) a shallow focus. The same area was struck on 1975 May 29 by another shallow earthquake (focal depth fixed at 0 km, $M_L = 4.2$, MSK VI) followed by two aftershocks.

These events are the only ones for which evidence clearly points to motion on the Vuache Fault. According to some catalogues (e.g. Amato 1983), seismic activity along the Vuache Fault in the last centuries would have been quite high, and most earthquakes felt in the Annecy area would be related to it. This would require that most historical events in the area—which tend to spread diffusely—were severely mislocated, which we doubt. Our compilation (Fig. 3) shows that only very few historical events may be confidently ascribed to the Vuache Fault itself, which has been rather quiet since the 17th century.

Recent microseismic activity along the fault is not very significant either. Since the mid-seventies, when the French, Swiss and Italian seismic networks have been able to detect any event with magnitude larger than about 2.5, very few shocks have been located in the area. The strongest event reached a magnitude of 3.0 in 1983, near the NW end of the Vuache Mountain. In 1994, the completion of Sismalp, a 44-station network run by the Observatoire de Grenoble for monitoring the seismicity of the western Alps, lowered the

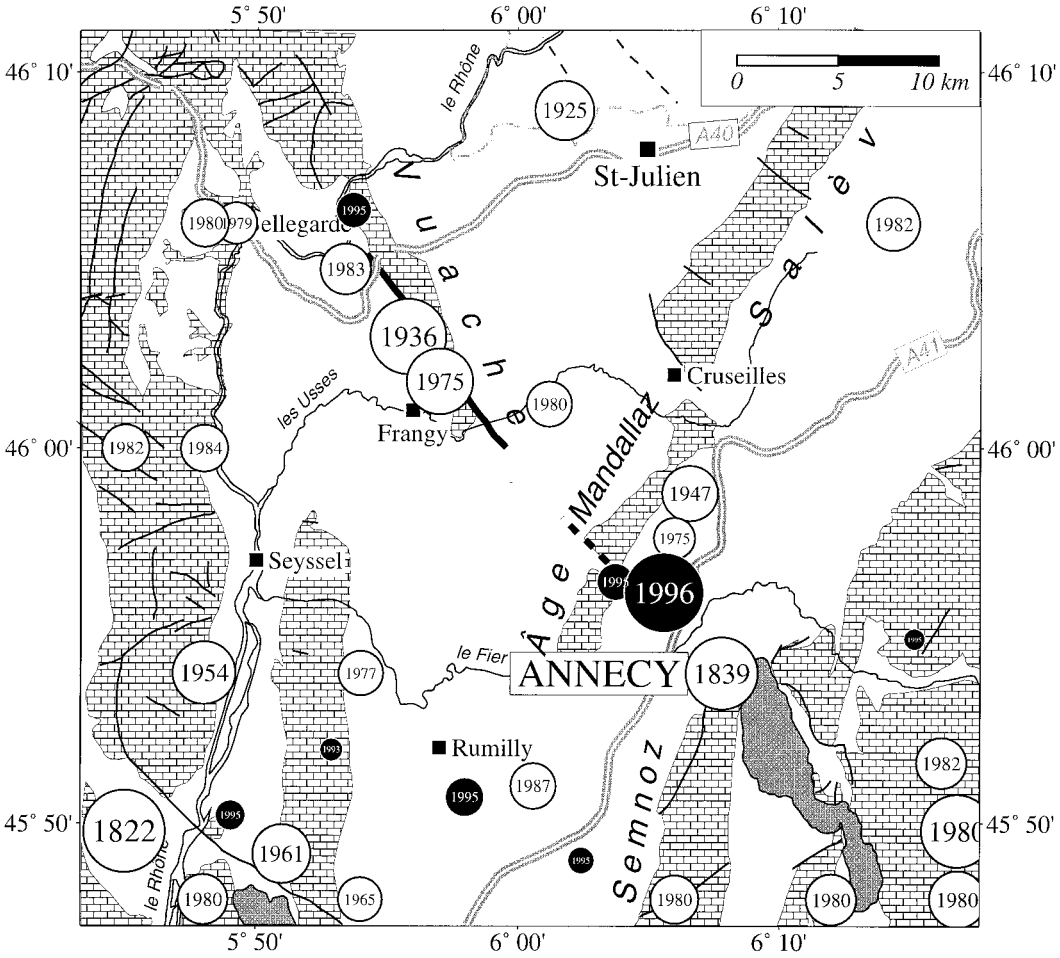

Figure 3. Seismicity of the Annecy region. See Fig. 1 for geographical location. Solid circles are earthquakes since 1988. Brick pattern indicates calcareous Subalpine chains (east) and Jura folds (west). Thick line is the surface expression of the Vuache Fault.

Table 1. 1-D minimum velocity model (Sellami et al. 1995) used for locating the main shock.

Depth (km)	P-wave velocity (km s^{-1})
0	4.85
1	5.90
3	5.95
5	6.00
10	6.25
15	6.30
20	6.50
30	6.65
38	8.25
50	8.27
60	8.28

Table 2. Local 1-D velocity model used for locating aftershocks.

Depth (km)	P-wave velocity (km s^{-1})
0	4
1	5.4
3.5	5.95
Below: same model as Table 1.	

detection level to a magnitude of about 1.5. Even so, only two events have since been recorded, both in 1995, with magnitudes slightly less than 2: the first struck close to the 1983 epicentre; the other, on 1995 August 2, was within 2.5 km of the 1996 epicentre, at 1 km depth. Whether or not this event may be considered an early 348-day foreshock of the 1996 15 July earthquake is debatable. The unusually long aftershock sequence that followed the main shock—two years later, aftershocks are still recorded and even felt—makes this hypothesis likely.

THE MAIN SHOCK

Location

The main shock of 1996 July 15 struck at 00:13:30 UTC (02:13:30 local time), just after the end of the Bastille Day festivities. Had it happened two hours earlier, casualties might have been quite high, given the dense crowd in the streets of Annecy and suburbs, where many chimneys collapsed. Luckily, only one slight injury was reported. Most of the damage occurred in the ancient part of the city and in its NW suburbs (Epagny, Metz-Tessy, Meythet, Poisy, Pringy; see Fig. 2a), where several churches were subsequently closed owing to the need for extensive repairs. The Epagny church and the nearby town hall were damaged beyond repair and will have to be demolished. In Meythet, 50 inhabitants living in a four-storey building constructed at the end of the sixties had to be evacuated because of the presence of X-cracks in the side walls of the two lowermost floors. According to the Bureau Central Séismologique Français, the maximum intensity reached was MSK VII–VIII within a 50 km2 area (Fig. 1). The total loss from damage to buildings amounted to 300 million French francs (about $50 million), the highest amount due to an earthquake in France for many years. The shock was felt all the way to Grenoble (85 km away, I = III–IV) and Lyons (100 km away, I = III).

The focal parameters of the main shock were computed using data from the French, Swiss and Italian networks (Fig. 1). The epicentre is located well within the Sismalp network. 33 stations with epicentral distances shorter than 150 km were selected for locating the earthquake, in order to rely only on crustal phases. In this way, residuals are not biased by strong Moho depth variations affecting mantle phases. We ran a version of the HYPO71 program (Lee & Lahr 1975) modified at the Observatoire de Grenoble to take into account elevation corrections and secondary arrivals. The velocity model of Table 1 (Sellami et al. 1995) was first used to locate the hypocentre. In a second stage, we performed a relative location using a local velocity model (Table 2), after enough aftershocks had been recorded by both the permanent network and the temporary network set up the day after the main shock. Assuming that the temporary network provided the most accurate locations, mean P-wave residuals from the strongest aftershocks were computed for the stations of the permanent network, and these residuals were thereafter subtracted from arrival times observed for the main shock. The relocation falls within 1.3 km of the first estimate (see focal parameters in Table 3), for a focal depth fixed at 2 km below sea level. Testing different focal depths shows that the focus is definitely very close to the surface, and therefore within the post-Triassic sedimentary sequence that covers the 3.5-km-deep basement. (A depth below sea level to the pre-Triassic basement of 3352 m is documented in the Chapery borehole, close to Rumilly, 15 km to the SW.) Horizontal and vertical uncertainties for the main shock are discussed in detail in the next section of this paper.

The epicentral area lies 4 km NW of Annecy, at the limit between the three districts of Epagny, Metz-Tessy and Meythet. This is a flat area known as 'Plaine d'Epagny', filled by fairly thick lacustrine clays during postglacial warming (since about 14 ka). This 15 km2 swamp zone was completely drained only 50 years ago and now accommodates the airport and a commercial park. Site effects due to the clay deposits are discussed at the end of this paper.

Magnitude and seismic moment

Magnitude estimates vary significantly according to national or international agencies. In Table 4, they range from 4.2 to 5.3. The m_b magnitude value computed with stations at large epicentral distances could be expected to match the M_L value since the m_b scale can be considered an extrapolation of the M_L scale for moderate-magnitude events. Available m_b values are less than 4.5, which might indicate that the LDG/CEA

Table 3. Location parameters for the main shock. ERH = Horizontal uncertainty; ERZ = Vertical uncertainty.

Date	Time (UTC)	Latitude	Longitude	Z (km)	ERH (km)	ERZ (km)
15.07.1996	00:13:30.0	45°56.3′N	6°05.3′E	2 (fixed)	0.7	3

Table 4. Magnitude estimates for the main shock. NDC = National Data Center for GSETT-3 (CHE = Switzerland, DEU = Germany, ESP = Spain, FRA = France, GBR = Great Britain, ITA = Italy); IDC = International Data Center for GSETT-3.

Agency	M_L	m_b
ITA–NDC	4.2	
ESP–NDC	4.3	
GBR–NDC	5.0	
CHE–NDC	5.1	
DEU–NDC	5.1	
ReNaSS	5.2	
FRA–NDC (LDG)	5.3	
IDC		4.17
USGS		4.5

value of 5.3 is an upper bound. However, we take it as a reference here, because over the last 35 years LDG has computed a long series of magnitudes for events in France and surrounding areas (Massinon 1979), which is the sole way to compare magnitudes between recent and past earthquakes.

Estimates of the seismic moment range from 2.6×10^{15} N m (Dufumier & Rouland 1998) to 8.5×10^{16} N m (G. Bock, personal communication, 1998), both values being computed using broad-band stations. Intermediate values of 1.2×10^{16} and 1.9×10^{16} N m were computed using accelerometric records from, respectively, the French Reseau Accelerometrique Permanent (Cornou 1997) and the Swiss accelerometric network, which operates a station only 30 km from the epicentre (F. Courboulex, personal communication, 1997). Using these seismic moment values, the Kanamori (1977) relation yields M_W magnitude values between 4.3 and 5.3.

Fault plane solution

The focal mechanism of the main shock was derived from the first-motion data recorded at 130 stations with good azimuthal coverage (Fig. 4). The solution is well constrained: slightly changing the velocity model or the focal depth does not modify the strike and dip values of the nodal planes by more than 5°–10°. However, a few discrepant observations in the SE azimuth, deflected by up to 20° from their original quadrant, correspond to clear crustal-path arrivals for stations with short epicentral distances (between 65 and 95 km), and we cannot discard them so easily. Strong lateral velocity variations might produce such ray deviations, but we cannot rely on those mapped in the Savoie region by the current 3-D tomography of the Alpine arc (Solarino et al. 1997) because this border region lacks resolution. A local NE updip of sedimentary and/or crustal interfaces beneath the focus is an alternative and more likely explanation.

The main shock had a clear strike-slip mechanism; within the uncertainty limits, it also displays a slight extensional component. The N50°E-striking nodal plane dips 80° to the SE, while the N136°E-striking plane dips 70° to the NE. The N50°E direction is that of the Alpine frontal thrust and, to a lesser extent, of the Jura internal folds and thrusts (Fig. 1). However, the N136°E nodal plane strikes almost parallel to the Vuache Fault (local strike: N135°E), which implies that it should be taken as the fault plane. Motion on this plane would thus have been left-lateral. The aftershock distribution and

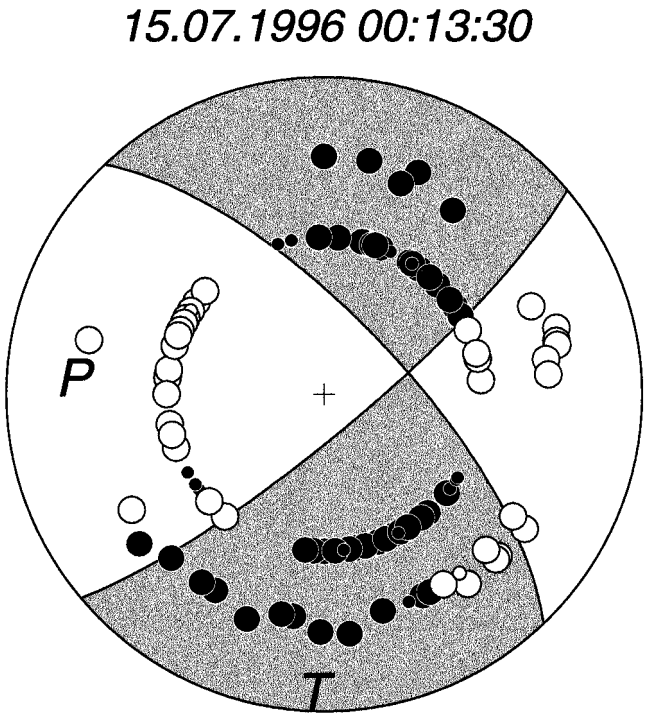

Figure 4. Focal mechanism of the main shock (lower-hemisphere Schmidt projection). Full symbols: compression; open symbols: dilatation; symbol size is smaller when first motion is emergent. Preferred fault plane strikes N136°E, with a 70°NE dip.

Table 5. Focal-solution parameters for the main shock. Strike, dip, and rake as defined by Aki & Richards (1980). Focal depth fixed at 2 km. Velocity model is that of Table 2. Preferred fault plane in bold type.

	Strike	Dip	Rake
Plane 1	50°	80°	−160°
Plane 2	**316°**	**70°**	**−10°**
	Trend	**Plunge**	
P axis	274°	22°	
T axis	181°	7°	

their focal mechanisms (see below) will substantiate this choice. The T-axis is nearly horizontal, with a N–S trend, while the P-axis trends E–W, with a 22° plunge to the west (Table 5).

In the region where the Epagny earthquake occurred, few reliable fault plane solutions are available (Frechet 1978; Sambeth 1984; Sambeth & Pavoni 1988; Menard 1988; Nicolas et al. 1990; Frechet et al. 1996). Most of them show anticlockwise rotation of the P-axis from a NW–SE direction in the southern Jura Mountains to a more E–W direction in the northern Subalpine chains. The P-axis orientation found for the Epagny earthquake is therefore characteristic of that generally observed in the Subalpine chains.

Because of the relative seismic quiescence of the Vuache Fault since 1936, only three fault plane solutions have been computed for events along the fault (Frechet 1978; Sambeth 1984; Sambeth & Pavoni 1988). All three are strike-slip mechanisms, consistent with a left-lateral slip on a

N105°E–N170°E-striking plane. The fault plane solution for the 1995 M_L 1.9 'foreshock' also indicates clear left-lateral strike-slip motion on a N145°E-striking plane.

Bock (1997) performed the only moment tensor inversion available to date for the Epagny earthquake. Using surface waves recorded by broad-band stations in Germany, Spain, Luxembourg, the Netherlands and Italy, he derived a normal-faulting mechanism, with N–S extension and only a minor strike-slip component. Aware of the discrepancy with the P-polarity mechanism, he discussed two possible reasons for it: (1) a change in the faulting mode where initial strike-slip changed into normal-faulting rupture, which is rather unlikely for a moderate-magnitude earthquake with a short rupture time; or (2) a 10-fold amplification of Rayleigh waves in the northerly azimuth, which may have been caused by strong lateral heterogeneities in the crust and the upper mantle along the propagation paths. This amplification might also explain the high values Bock inferred for the seismic moment and the corresponding M_W magnitude.

AFTERSHOCKS

Aftershock monitoring

Aftershock activity is difficult to monitor after moderate-magnitude earthquakes. For instance, the 10-km-deep M_L 5.1 Le Grand-Bornand earthquake (Frechet et al. 1996) was followed, 47 min later, by an M_L 2.8 faintly felt aftershock. 13 aftershocks of much lower magnitude (between −0.3 and 0.9) were recorded in the following 15 days. The activity then stopped, although we detected an isolated M_L 2.1 non-felt aftershock more than 13 months later. In contrast, however, during the two years following the M_L 5.3 Epagny earthquake, several hundred aftershocks were recorded, and more than 80 were felt. The strongest (M_L = 4.2) occurred on July 23, eight days after the main shock.

It was possible to monitor aftershocks thoroughly thanks to a temporary network of digital seismic stations that was swiftly deployed in the epicentral area. 10 stations with 2 Hz vertical seismometers were installed on July 15 within 4 km of the epicentre; four three-component stations completed the network two days later, as well as two more one-component stations (Fig. 5). For all stations, we used a permanent GPS-synchronized clock. The complete network was operated until July 29, when it was replaced by a lighter monitoring system, with seven one-component stations focused on the most active aftershock zone. This network was operated until the end of September. At the end of July and the beginning of August, we also used data from a six-station strong-motion network, also fitted with a GPS-synchronized clock. In addition, aftershocks with magnitudes greater than about 0.5 were recorded by the Sismalp network and by other national networks in France, Italy and Switzerland.

Several hundred aftershocks were recorded. We could locate

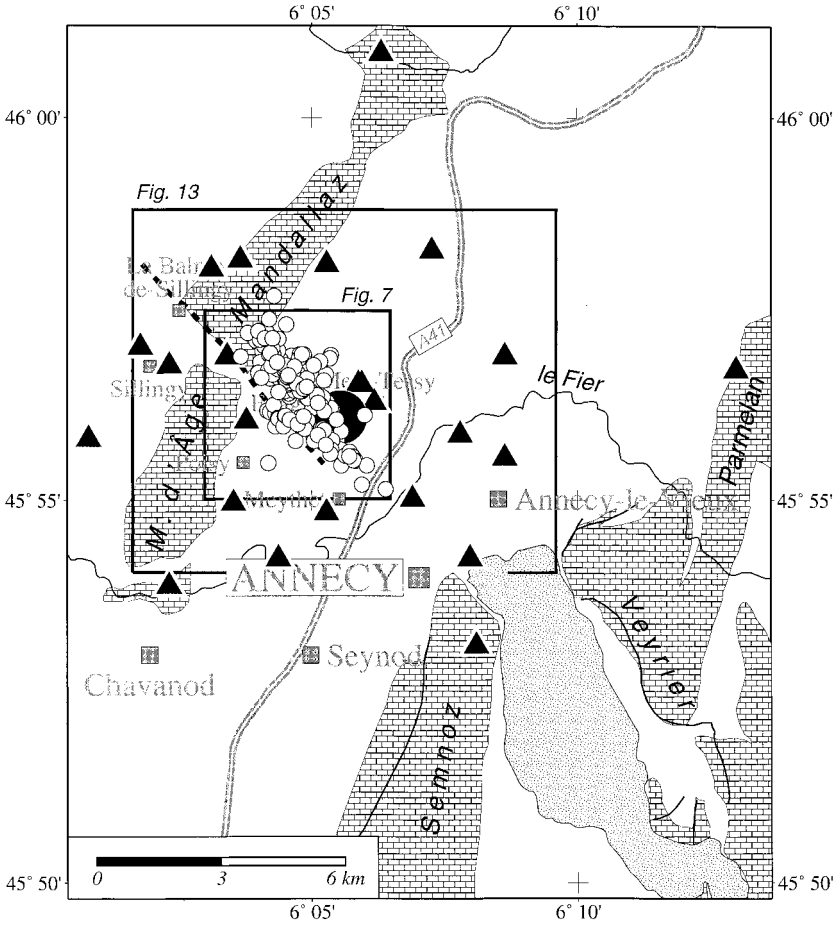

Figure 5. Map of the best located events in the aftershock sequence. Triangles indicate position of temporary seismic stations. Brick pattern symbol as in Fig. 3.

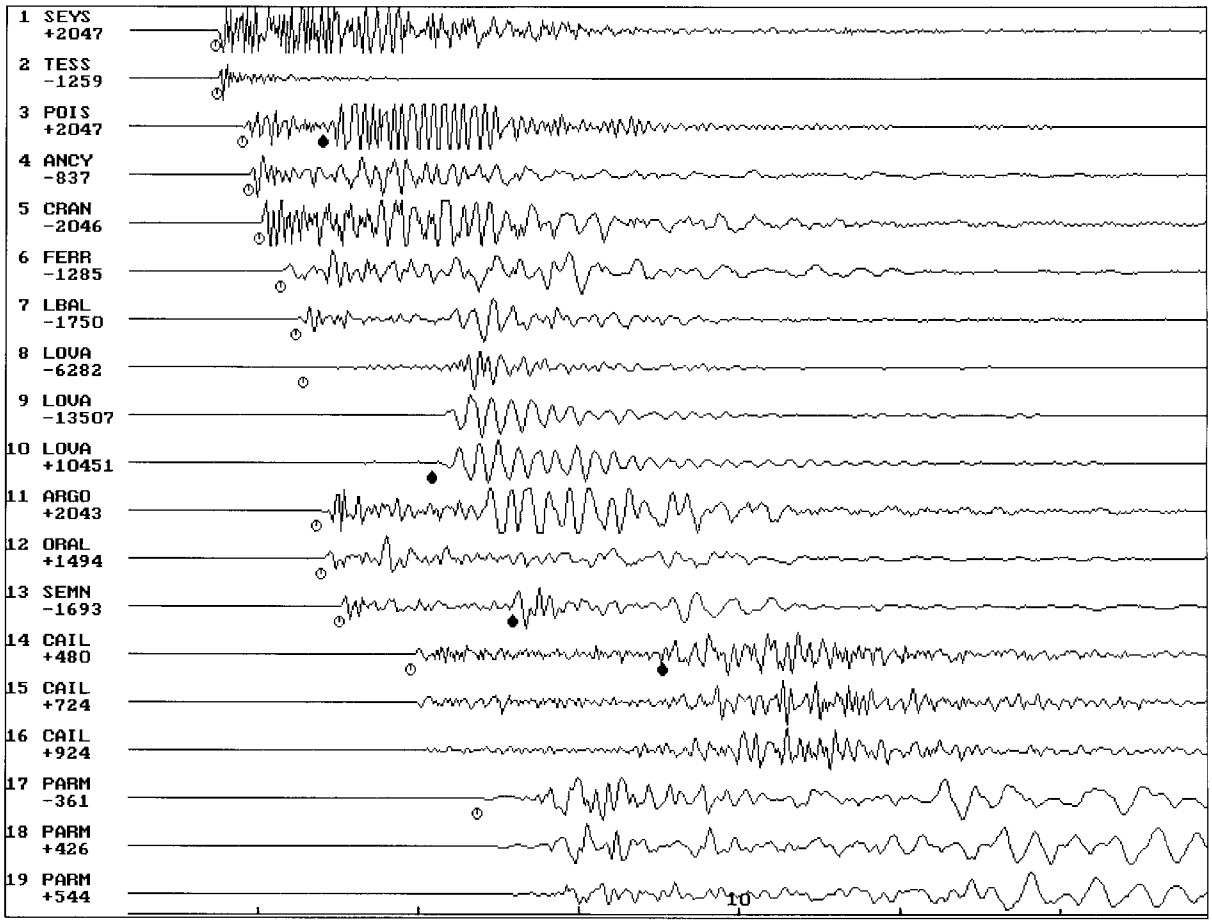

Figure 6. Example of a screen display with amplitude-normalized signals recorded by 10.2 Hz vertical-component stations and three 2 Hz three-component stations for an M_L 1.1 aftershock (focal depth 1.2 km). Three-component signals (stations LOVA, CAIL and PARM) are displayed in the following order: vertical, NS and EW. Tick marks at bottom indicate seconds. Epicentral distances range from 1.4 km (top) to 10 km (bottom). Flags show picked arrivals (open circles = P waves; full circles = S waves). Note the poor quality of S waves, which can often be mistaken for surface waves (signals #7 and #11). Three-component station PARM (three lowermost signals) did not record usable S waves.

about 400 events using our modified version of the HYPO71 program, with the local velocity model of Table 2. (We chose a V_P/V_S ratio of 1.71.) We select here 174 events whose locations can be considered as best constrained (i.e. with more than eight arrival times available, with azimuthal gap smaller than 180°, with epicentral uncertainty smaller than 300 m, and with depth uncertainty smaller than 500 m). Uncertainties are on average much smaller: 160 m in the epicentre, and 200 m in focal depth. On average, the RMS residual is 30 ms, and the epicentral distance to the closest station is 1.7 km.

With such a close and dense network, still smaller uncertainties could have been expected. The main problem was the poor quality and occasional absence of S waves (Fig. 6). This can be ascribed to the very shallow focal depths and to the low-velocity surface sediments that generate energetic surface waves easily mistaken for S waves, a ground-roll phenomenon visible even at short distances. Unexpectedly, picking S waves on three-component records was not much easier than on vertical-component records, regardless of the epicentral distance.

Aftershock distribution

The aftershock zone stretches in a NW–SE direction across the 'Plaine d'Epagny' (Fig. 7), along and close to the inferred continuation of the N135°E-striking Vuache Fault towards the SE, and under the lacustrine clay deposits of this plain. There is also good agreement between the N130°E trend of this zone and the N136°E strike of the fault plane deduced from the focal mechanism. The total length of the aftershock zone is about 5 km.

Focal depths range from 0 to 4.7 km below sea level, with a mean value of 2.2 km and a most probable value of 2.7 km. 96 per cent of the aftershocks occurred within the 3.5-km-thick post-Triassic cover (Fig. 8), mostly within the second layer of the local velocity model, which corresponds to the Upper Jurassic (Tithonian) and Lower Cretaceous (Urgonian) series. Where these series are exposed, as in the Mandallaz or Age mountains, they are mostly composed of massive, thickly bedded, erosion-resistant reef limestones that may indeed exhibit brittle behaviour at depth.

At a more detailed level, two elongated seismic clusters may be separated on the map and cross-section (Figs 7 and 8a). The northern cluster, with the main shock at its SE end, was the most seismically active, and it extends over about 4 km. It probably defines the main rupture plane. The northern cluster is separated by 500–800 m from the southern cluster, which was much less active, and whose NW end is marked by the 1995 'foreshock'. The separation of the two clusters is much

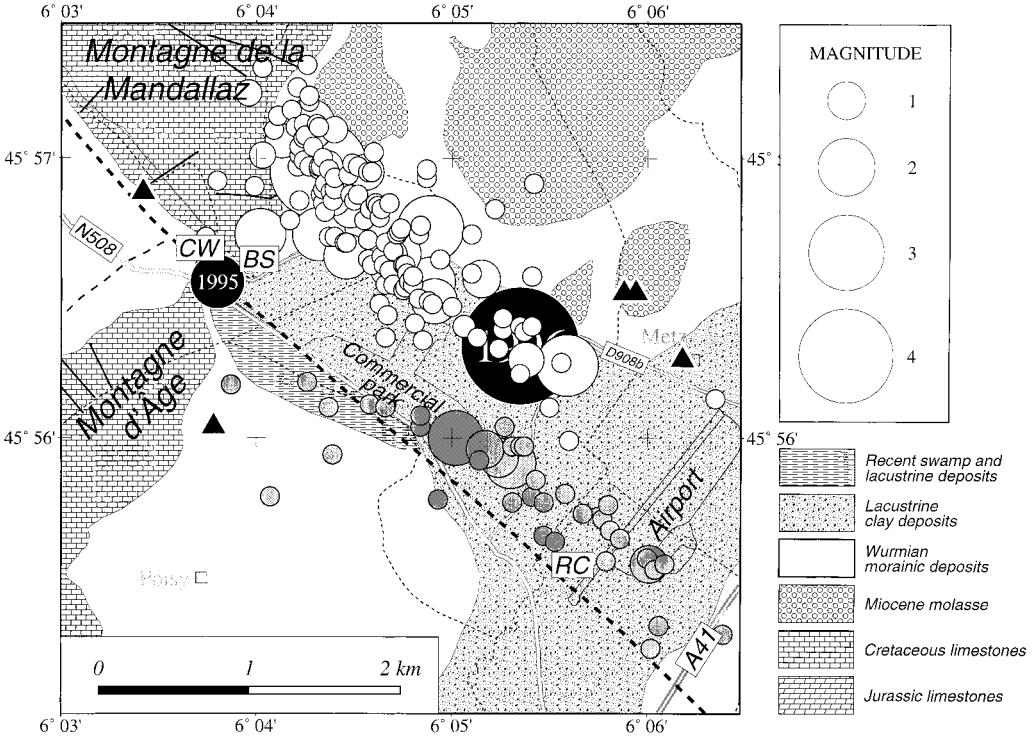

Figure 7. Aftershock map. Solid circles indicate epicentres of the main shock and of the 348-day 'foreshock', open circles those of aftershocks along the northern segment, shaded circles those of aftershocks along the southern segment. Solid triangles are temporary seismic or accelerometric stations. RC = runway cracks (Figs 11a and b), CW = Chaumontet warehouse (Fig. 11c), BS = Bromines spring (Fig. 11d). Light dashed lines are district boundaries. Thick dashed line is the inferred extension of the Vuache Fault, as shown on geological maps published prior to the 1996 earthquake.

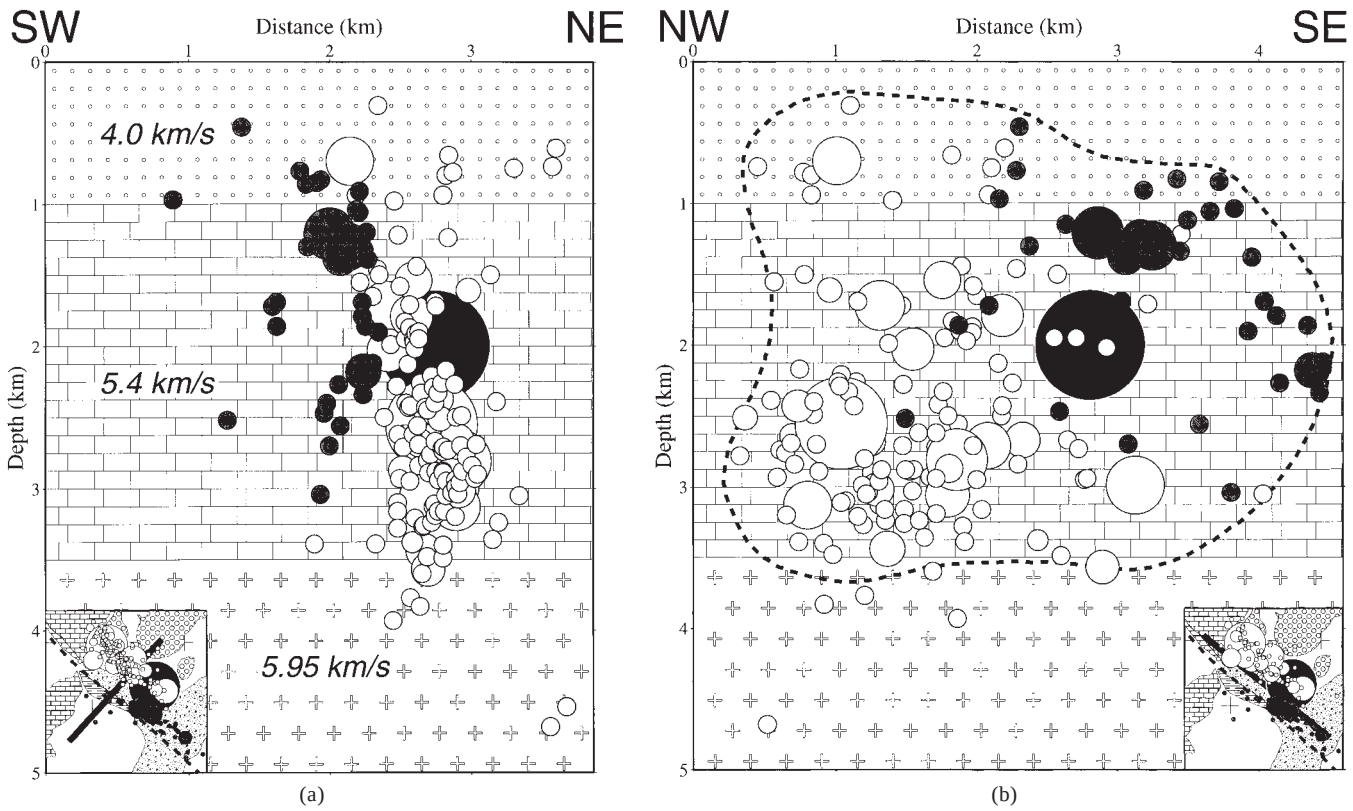

Figure 8. Sections across the aftershock zone. Symbols as in Fig. 7. (a) SW–NE cross-section of fault zone (velocity model is that of Table 2). (b) Along-strike NW–SE section. Thick dashed line is the inferred extension of the 10 km2 rupture surface.

larger than the mean epicentral uncertainty (160 m), which would suggest a distinct, somewhat shallower rupture plane, parallel to the main one. The southernmost plane projects to the surface along the limit between the wettest, possibly most subsident part of the Epagny marsh ('Marais Noirs') and the Oligo-Miocene molasse that forms the basement of the Poisy terrace. It also projects near the surface cracks (RC on Fig. 7) found near the SW tip of the Annecy–Meythet airport runway (Figs 11a and b).

The main fault plane has a 73° NE dip, consistent with the 70° NE dip derived from the focal mechanism. The dip of the southern plane is ill-defined: fitting the largest-magnitude hypocentres yields a 75° NE value. This plane may have acted as a south- and up-stepping splay of the main fault, allowing upward propagation of rupture to shallow depth.

A NW–SE along-strike section (Fig. 8b) yields an image of the fault patch ruptured by the earthquake. From this section, we estimate the rupture surface to be 10 km2. Given the seismic moment of about 3×1016 N m, and taking a mean rigidity of 25 GPa (consistent with a V_S velocity of 3.1 km s^{-1} and a density of 2600 kg m^{-3}), we estimate the average slip to have been 12 cm.

Main shock versus aftershocks

The main-shock position, computed by using permanent stations only, is not as accurate as that of the aftershocks (horizontal uncertainties of 700 m versus 160 m), and the rupture process cannot be understood without a proper discussion of these uncertainties. As the main aftershock (23.07.1996 04:08, $M_L = 4.2$) was recorded, up to 150 km away, by most of the permanent stations that recorded the main shock, we used the corresponding arrival times to relocate this aftershock with the same procedure as that used for the main shock, and to compare the solution with the 'true' position given by the temporary network. To simulate better the way the main shock had been recorded, we also stripped aftershock arrival times of most S-wave data, keeping only five S-wave arrival times for stations between 70 and 150 km away. As explained in the previous section, the first step was to locate the main shock and the main aftershock using the velocity model of Table 1 (Fig. 9a). In a second step, after enough aftershocks had been recorded by both the permanent network and the temporary network, we computed station corrections and used the local velocity model of Table 2. As a vertical uncertainty of several kilometres was computed for both events, it seemed sounder to set the focal depth at 2 km, a value close to the average focal depth for the aftershocks (2.2 km). For the main aftershock, the relocated epicentre falls within 300 m of the 'true' epicentre, with a horizontal uncertainty of 700 m. This substantiates the position obtained for the main shock, and the corresponding 700 m horizontal uncertainty.

Further information is provided by observations at station RSL. At a N124°E azimuth (close to the N135°E fault strike, see Fig. 9a) and an epicentral distance of 50 km, RSL is one of the few stations that recorded unclipped signals of the main shock with a three-component seismometer (natural frequency of 1 Hz). When the corresponding P waveforms are superimposed on those recorded for the second strongest aftershock (star in Fig. 9a), we observe a clear shift of about 0.1 s for the S waveforms (the S waveform is earlier for the main shock). As this analysis is carried out on the waveforms, the corresponding difference in the ray path geometry is relative to the centroids (optimal point-source locations for the seismic moment release). For the second strongest aftershock ($M_L =$ 2.5, focal depth 3 km), the hypocentre (the place where the rupture initiated) and the centroid (the barycentre of slip

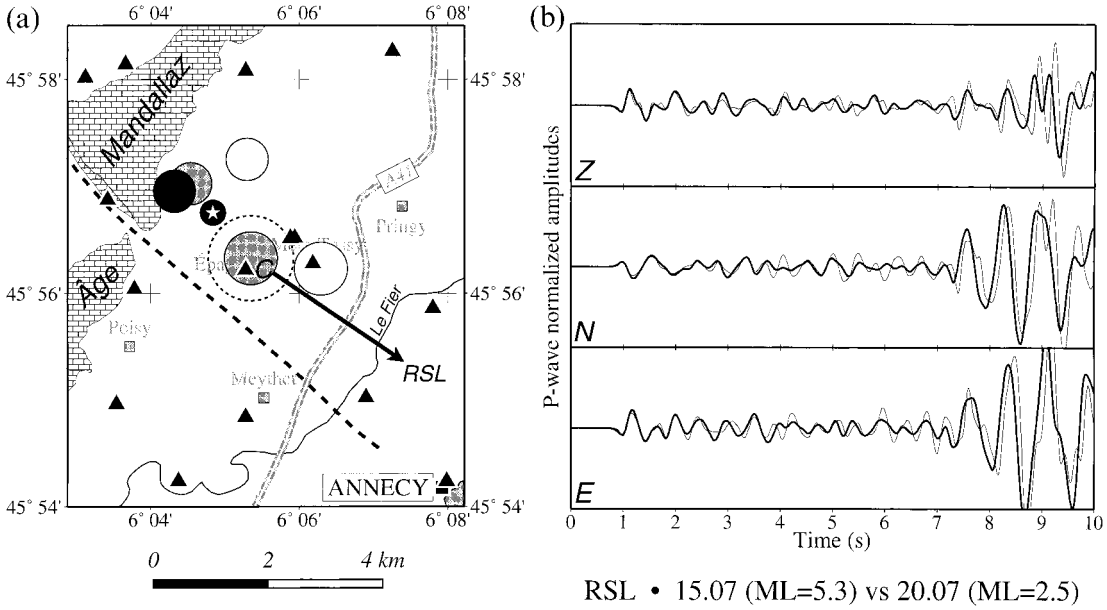

Figure 9. (a) Testing the location accuracy of the main shock and main aftershock using permanent stations. Standard locations shown as open circles; locations using station corrections shown as shaded circles. Dotted circle around main-shock epicentre shows epicentral uncertainty. For the main aftershock, the epicentre computed using data from the temporary network is shown as a solid circle. Epicentre of the second largest aftershock shown by a star. C = Position of the main-shock centroid (see text). Station RSL, at a N124°E azimuth and a distance of 50 km, recorded the signals shown in (b). Thick dashed line is the inferred extension of the Vuache Fault. (b) 0.1–2.5 Hz bandpass-filtered signals recorded by the three-component short-period station RSL for the main shock (thick line) and the second largest aftershock (thin line). P waveforms are superimposed and scaled. The S waveform is earlier by about 0.1 s for the main shock.

distribution on the fault) can be considered as being practically in the same place, since the expected source radius for an M2.5 earthquake is of the order of 100 m. Assuming a 2 km depth (in the middle of the Mesozoic series) for the main-shock centroid, the 0.1 s time shift observed at station RSL locates the centroid 1.2 km to the SE of the aftershock. (This computation takes into account the 1 km difference in focal depth between the two sources.) The main-shock centroid falls within 300 m of the epicentre (Fig. 9a), and we conclude that the rupture was primarily bi-directional (towards the NW and SE). We must admit, however, that shifting the main-shock epicentre within its uncertainty domain can also provide a significant asymmetry in the rupture process.

However, if the rupture propagated in both directions, Fig. 7 shows only very few aftershocks on the northern fault plane SE of the main shock. If the above chain of reasoning is correct, the only explanation is that the rupture cleared the barrier between the two planes and continued towards the SE along the southern fault plane. The main-shock position, at the SE end of the northern cluster and close to the NW end of the southern cluster, is perhaps no coincidence.

Finally, the aftershock concentration to the NW, close to the SE flank of the Mandallaz Mountain, might provide an indication that this mountain acted as a barrier that prevented the rupture from propagating farther to the NW. Here, the 1–3.5-km-deep Mesozoic series is abruptly brought up to the surface in mighty folds, which might modify the stress state in these layers, in which most of the aftershock activity occurred.

The above analysis provides no information on the focal depth of the main shock. The 2 km value we chose locates the hypocentre in the middle of the Mesozoic series. We observe a dramatic increase in the rms residual when the focal depth is set at a deeper level, the best fit actually being obtained for 0 km depth. As this would have produced extensive surface phenomena, which were not observed, and as a vertical uncertainty of 3 km was computed, we conclude that the focus is definitely very shallow, but deep enough to produce only faint surface breaking. Therefore, the 2 km value we chose results from this trade-off, with three additional observations being taken into account: (1) most aftershocks occurred around that depth; (2) the fault plane solution shows fewer anomalous polarities when the focus is deepened from 0 to 3 km; and (3) sPn depth phases observed by Bock (1997) on broad-band records yield a focal depth of 2–3 km.

Fault plane solutions

The temporary stations were close enough to the epicentres that a number of focal mechanisms can be derived, even for small-magnitude aftershocks. In Fig. 10, we selected 60 fairly well-constrained focal mechanisms computed using the FPFIT program (Reasenberg & Oppenheimer 1985). Most of them show strike-slip motion, with nodal planes striking NW–SE and SW–NE. If the NW–SE-striking plane is chosen as the fault plane, most aftershocks exhibit left-lateral slip, consistent with that in the main shock. A few aftershocks display normal faulting with a N–S-trending T-axis, consistent with a component of N–S extension and the moment tensor solution of Bock (1997). Still fewer solutions exhibit a component of reverse faulting with an E–W-trending P-axis.

EFFECTS OF THE MAIN SHOCK

Rupture traces and surface phenomena

Despite the moderate magnitude, M_L 5.3, of the main shock (and a still lower value for m_b), rupture may have reached the

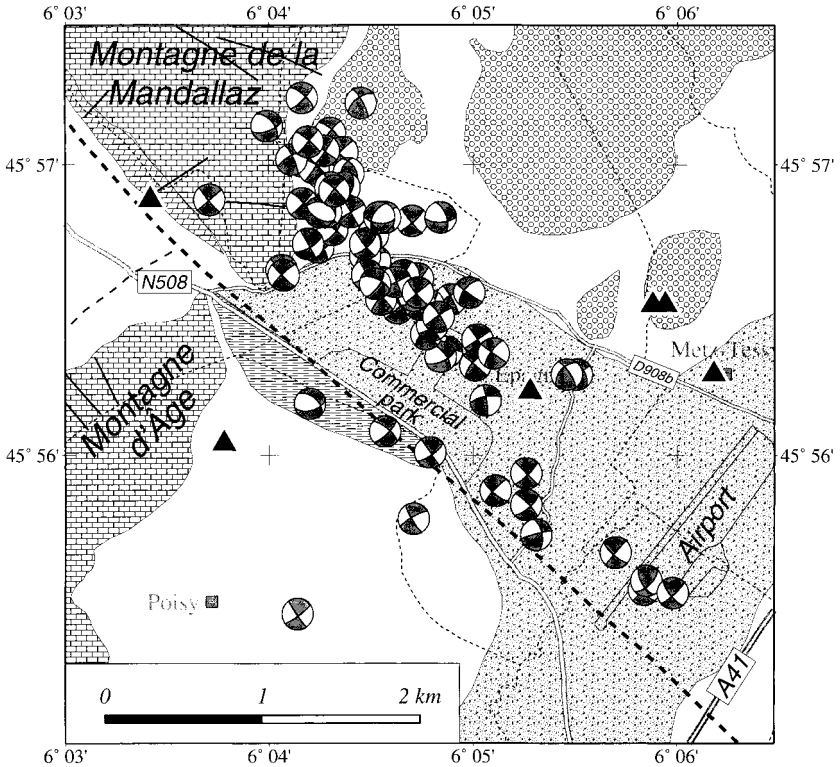

Figure 10. 60 aftershock fault plane solutions. Most resemble that of the main shock (Fig. 4); a few imply components of roughly N–S extension.

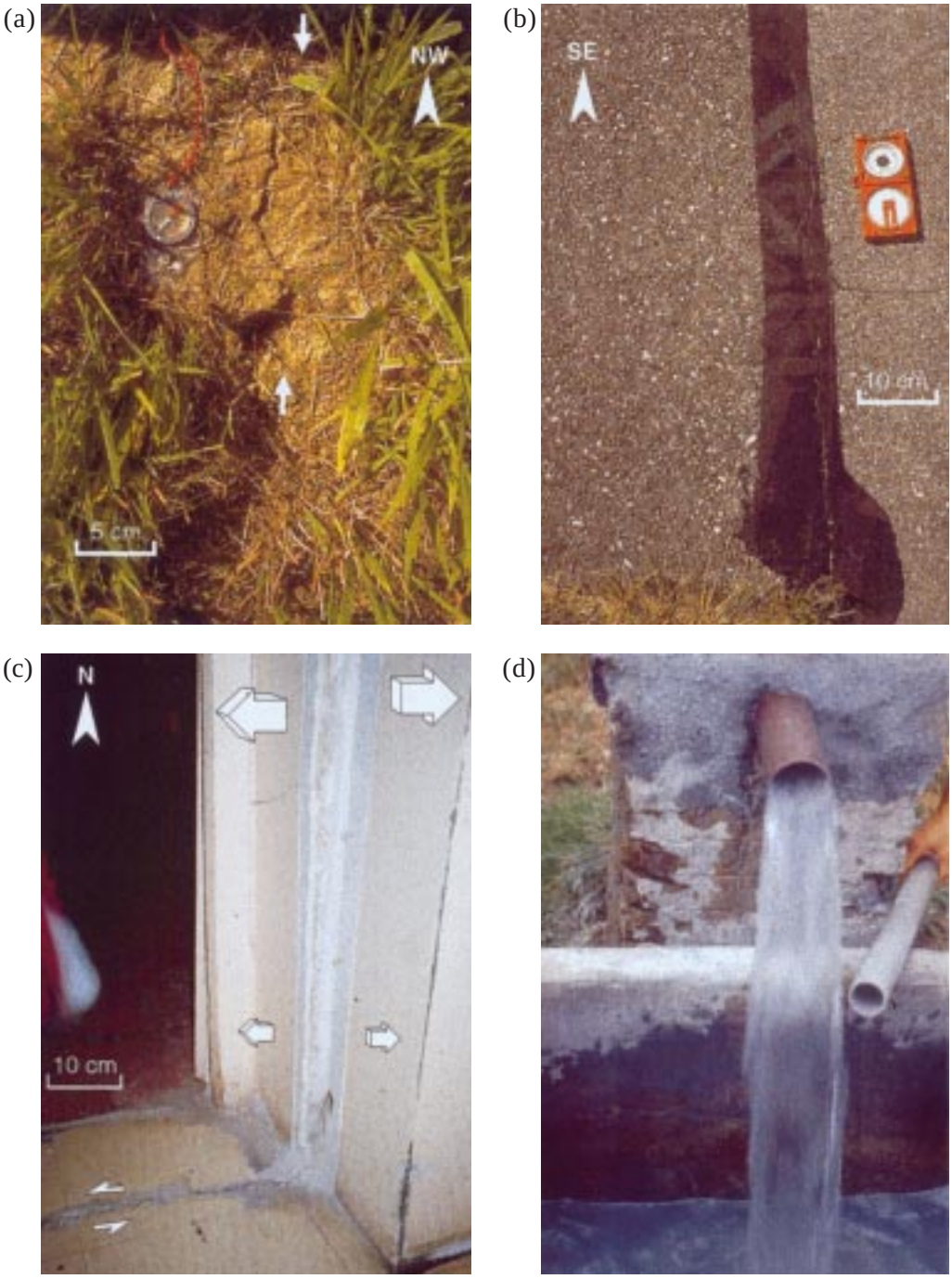

Figure 11. Ground cracks (a) a few metres west of and (b) on the runway of the Annecy–Meythet airport; see Fig. 7 (RC) for location. (c) Left-lateral strike-slip displacement at the Chaumontet warehouse; see Fig. 7 (CW) for location. (d) Output increase at Bromines spring, with old pipe and new pipe; see Fig. 7 (BS) for location.

surface because of the particularly shallow focal depth. Other surface phenomena possibly related to shallow deformation were also observed.

Just off the runway of the Annecy–Meythet airport, 1.7 km SSE of the epicentre (Fig. 7), we found N140°E-striking cracks in the ground (Fig. 11a). Two days after the earthquake, the cracks had openings of 1–3 cm. Although such cracks might result from summer desiccation of the ground, the fact that we could follow them for about 200 m, parallel to the Vuache Fault, across a completely flat area convinces us that they were induced by a small relative displacement of the soft shallow sediments due to slip on the fault below. Moreover, the cracks lie precisely in the area where the fault plane, deduced from the location of the shallowest aftershocks, might be extrapolated to intersect the ground surface. Fresh cracking of 1 or 2 mm of a recent bituminous joint transverse to the runway was also observed in near continuation with the ground cracks (Fig. 11b).

At Chaumontet, a locality situated 2 km NW of the epicentre, near the expected Vuache Fault trace (Fig. 7), at the foot of

the SW flank of the Mandallaz Mountain, we found horizontal displacement within the structure of a warehouse, at the join between the main building and its annex (Fig. 11c). In the concrete floor, we observed a left-lateral displacement of a few millimetres up to 1 cm, associated in places with en echelon secondary cracks. There was also a 1 cm uplift of the northern part of the building relative to its southern part. Although the corresponding crack zone trends E–W, and is hence not parallel to the N135°E-striking Vuache Fault, the left-lateral slip is compatible with the focal mechanism. The deformation observed might thus be partly induced by fault slip, and modified by the structural response of the building (Jalil & Bisch 1997).

Flow changes in two natural springs close to the epicentre were noted. The otherwise very steady Bromines sulphurous spring, at the foot of the southern tip of the Mandallaz Mountain (Fig. 7), is reported to have significantly increased its flow just after the earthquake. This increase was strong enough to partially damage the spring harnessing, and a new pipe with a diameter twice as large as the old one had to be installed (Fig. 11d). Though no flow measurement before the earthquake is available, we can estimate from the pipe diameters that the water flow increased by a factor of 4 or 5. One year after the main shock, the flow was still greater than normal. Conversely, another non-sulphurous spring located 1 km to the north of Bromines was reported to have run dry just after the earthquake. It recovered its initial flow only 4 months later. Underwater springs in the northern part of Lake Annecy were also said to have increased their output following the earthquake, but this information was not verified.

Geodetic levelling

Within the framework of the Climasilac programme (a study of Lake Annecy and of its drainage area), geodetic routes levelled by the Service Geographique de l'Armee in 1902 and by the Institut Geographique National in 1979 were partly re-levelled in 1994, mainly along Lake Annecy. After the 1996 Epagny earthquake, data from several levelling campaigns carried out in 1996 and 1997 became available for this study.

Fig. 12(b) shows vertical movement along a roughly NW–SE route that skirts around the north of the 'Plaine d'Epagny' (Fig. 12a). Unfortunately, survey sites in the epicentral area were not re-levelled in 1994, so these data represent elevation changes between the 1979 and 1996–1997 surveys and cannot be considered coseismic. However, there is a clear difference of 1–1.5 cm between the western (lower) and eastern (higher) parts of the profile. This drop occurs in the Bromines area, where the profile crosses the most active part of the aftershock zone.

To prove that these elevation changes are coseismic, we compared them with those measured along a roughly N–S route, about 5 km SE of the epicentral area (Fig. 12a), which was re-levelled in 1994. Fig. 12(c) shows that the relative movement that tended to lower the central part of the profile by about 0.5–1 cm between 1979 and 1994 drastically increased by more than 1 cm between 1994 and 1996–1997. Fig. 12(d) provides a long-term check of what can be considered a coseismic phenomenon: along the same profile, the relative velocity for the 1902–1979 period amounts to a few tenths of a millimetre per year, a value very similar to that for the

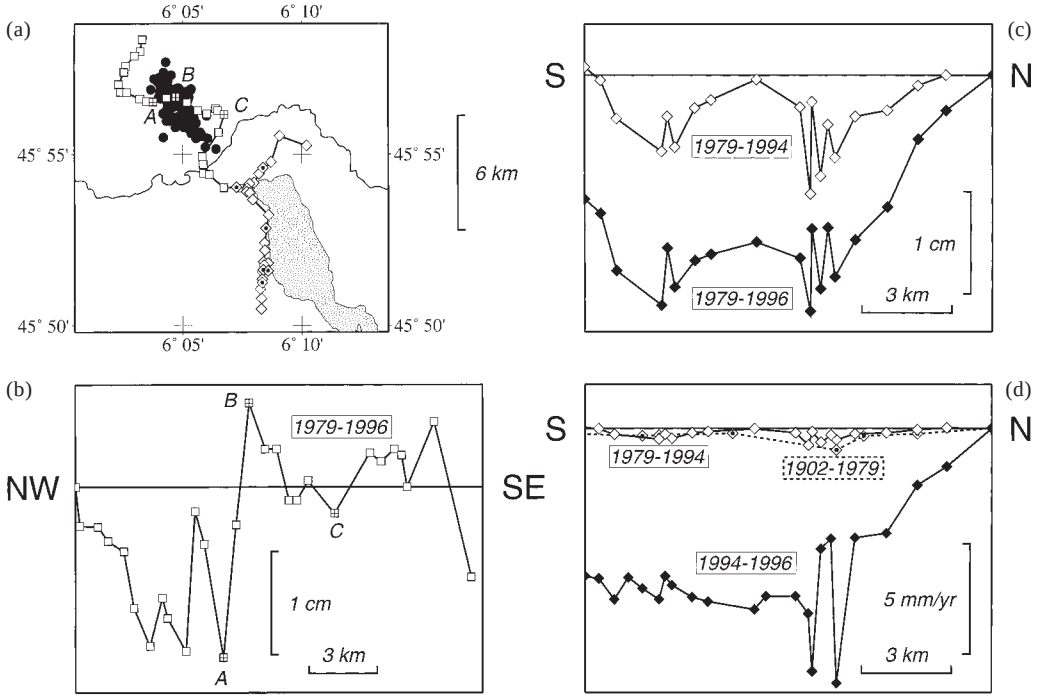

Figure 12. Levelling survey in the epicentral area. (a) Squares show the NW–SE profile (measured in 1979 and 1996–1997), diamonds show the N–S profile (measured in 1979, 1994 and 1996–1997), with sites also measured in 1902 marked with a dotted symbol. Black dots indicate the aftershock zone. A, B, and C (marked with crosses) are three sites close to the aftershock zone. (b) Vertical movements along the NW–SE profile. (c) Vertical movements along the N–S profile. (d) Vertical velocities along the same profile.

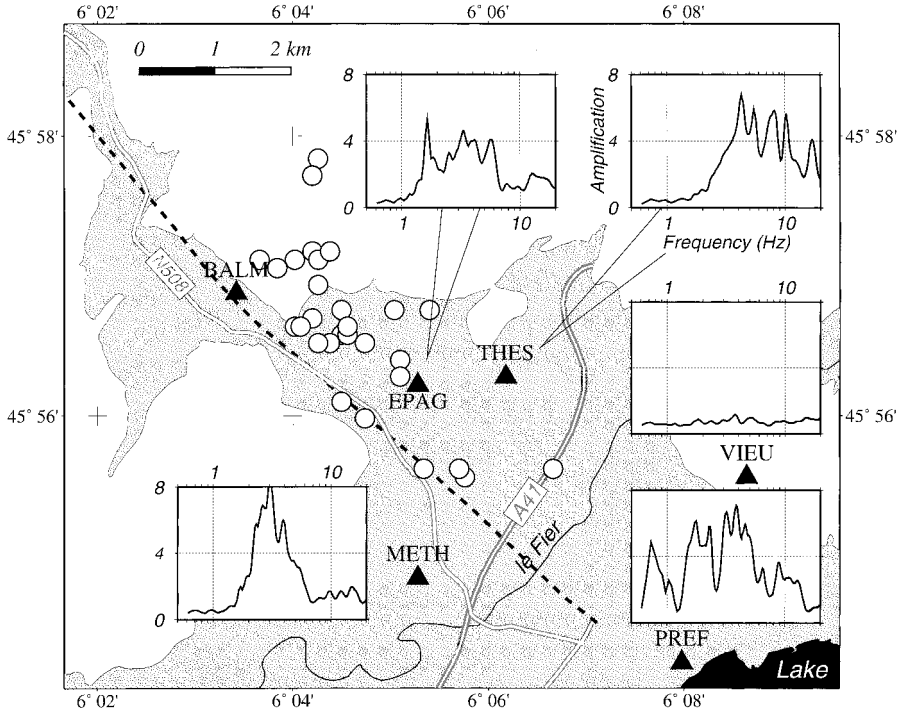

Figure 13. Site functions for five stations in the Annecy Basin (triangles). Shaded: topography lower than 500 m. Aftershocks used are shown with open circles. Station BALM, on Tithonian (Jurassic) limestone, is taken for reference. Only station VIEU, on molasse hills away from the Annecy Basin, shows amplification close to 1; other stations show amplifications of up to 8.

1979–1994 period, while it increases to more than 5 mm yr^{-1} within the 1994 to 1996–1997 two-year time span.

The uplift of the eastern part of the 'Plaine d'Epagny' relative to the western part (Fig. 12b), as well as that of the north of the profile in Fig. 12(c) relative to the south, are in the opposite sense to that of the vertical component of motion consistent with the fault plane solution: in Fig. 4, the fault plane dips to the NE, and if any vertical movement were observed, we would expect an uplift of the SW block relative to the NE block. Neither is the CMT solution (Bock 1997), with normal faulting on E–W-striking nodal planes dipping at 45°, consistent with the levelling observations: it would not explain the relative movement between points A and B (Figs 12a and b), since these points are E–W-oriented and will therefore be located on the same tectonic block. All things considered, Fig. 12(d) suggests an acceleration of vertical movement induced by the earthquake, rather than as a direct consequence of slip on the Vuache Fault.

Site effects

During the main shock, site effects clearly played a major role in the distribution of damage. In the city of Annecy, for instance, which is mostly built on lacustrine clay deposits that are also found in the 'Plaine d'Epagny', structural damage was much greater than in Annecy-le-Vieux, a NE suburb partly built on moraine and Tertiary molasse, in spite of similar epicentral distances and very close backazimuths (see Fig. 2a).

To study such site effects using aftershocks, we installed six three-component accelerometric stations between July 23 and August 3 (Fig. 13). One was set up on the bedrock of the Mandallaz Mountain to provide a reference, another was set up on the Annecy-le-Vieux hill, and the other four were installed on the flat alluvial plain of the Annecy Basin. To determine site effects, we used the generalized inversion method discussed by Field & Jacob (1993). By inverting signals recorded for 30 aftershocks, we obtained the source function of each aftershock and the site function at each station (Le Brun 1997; Riepl et al. 1998).

Fig. 13 shows the site functions for the five stations in the Annecy Basin. Station VIEU, located on the hill, where no extensive damage was reported, shows a spectral ratio close to 1 at all frequencies. Station PREF displays amplification even at very low frequencies, which can be explained by its proximity to the lake, with lacustrine deposits probably thicker than elsewhere in the basin. The other three stations show resonance peaks between 1 and 10 Hz, with up to eight-fold amplifications. The 1–5 Hz frequency range is precisely that of resonant frequencies of buildings, which probably accounts for the relatively heavy damage produced by an earthquake of such moderate magnitude.

DISCUSSION AND CONCLUSIONS

Perhaps the most striking feature of the seismicity along the Vuache Fault is the apparent quiescence of its middle segment, between the Mandallaz Mountain and the SE end of the Vuache Mountain (Fig. 3). No historical earthquakes have been reported along this 12-km-long segment, although we must re-emphasize how little we know of the pre-instrumental seismicity of the area.

If we postulate that the 1839 event was located beneath

Annecy, where it ruptured a few kilometres of the Vuache Fault, we can consider the 1996 event to have extended this rupture farther to the NW. Interestingly, this rupture was stopped by the Mandallaz barrier, whereas the 1936 event and, to a lesser extent, the 1975 event probably both ruptured the fault along the SE tip of the Vuache Mountain. Unless fault creep—for which we have little evidence at this time—is invoked, the Vuache–Mandallaz fault segment should be singled out as a likely site for other earthquakes with magnitudes comparable to that of the Epagny earthquake, or even for a single larger earthquake.

Since Omori (1907) first explicitly stated the seismic gap concept, it has proved deceptive in certain cases (Kagan & Jackson 1995). This hypothesis is normally applied to large earthquakes at plate boundaries, with fault dimensions of 100 km or more and fast slip rates (e.g. Gaudemer et al. 1995). In addition, according to Scholz (1990), one needs either positive evidence for a previous large earthquake or negative evidence for fault creep before identifying a given fault segment as a seismic gap. These pieces of evidence are clearly lacking, and we are well aware that considering the Vuache–Mandallaz segment as a seismic gap on a much shorter and slower-slipping fault is debatable.

However, given its length, and taking scaling laws into account (e.g. Scholz 1990), this 12-km-long segment could be ruptured by an event of magnitude up to 6, with about 20 cm of cumulative slip. With our very rough estimate of the slip rate (0.08–3 mm yr^{-1}), the recurrence time of such an event has large uncertainties, and lies anywhere between 70 and 2500 years. The lower figure is unrealistic, and shows that the 3 mm yr^{-1} value derived on geological grounds is much too high. The seismic history suggests that the recurrence time exceeds 200 years, and perhaps 600 years.

Another hypothesis would be that the 1839 event ruptured exactly the same fault patch as the 1996 event. We regard it as unlikely because damage after the 1996 earthquake was more severe than after the 1839 event. However, as the magnitude of the 1839 event was probably lower than that of the 1996 event, we cannot completely discard the hypothesis that both events occurred on the same fault segment and were separated by a recurrence time of about 150 years. Using the 12 cm slip supplied by the seismic moment estimate, this would imply a slip rate of 0.8 mm yr^{-1}.

The 1996 Epagny earthquake was remarkable, both in its magnitude of 5.3—an unusual value for a moderate-seismicity region—and in the many aftershocks felt for several months afterwards. (Nearly two years after the main shock, aftershocks of $1 < M_L < 2$ are still felt.) More significantly, this is the first time in the western Alps that detailed mapping of a rupture plane has been achieved and that aftershocks have been unambiguously linked to a visible surface fault. We probably owe this success to the shallow focal depth of the main shock and to the tectonics of the epicentral area, perhaps simpler than elsewhere in the Alps: at least on large-scale tectonic maps, the Vuache Fault appears as one single, well-identified, major fault.

On a smaller scale, this study shows that, even for a moderate-magnitude event, the rupture geometry can be complex. We identified two parallel fault planes splaying 500–800 m apart. Fault plane solutions for aftershocks on both fault planes mainly indicate strike-slip mechanisms. This can occur only if there is a barrier between the fault planes. Events close to this barrier also have strike-slip mechanisms. We did not find any normal- or reverse-faulting events in this zone. The Mandallaz Mountain was another barrier that possibly prevented the rupture from propagating farther to the NW.

We reported several surface observations following the main shock. None of them alone would be sufficient for drawing robust conclusions, but all are consistent with the results derived from the seismological study. Only the levelling data appear to be inconsistent with the almost pure strike slip inferred from the fault plane solution. A complex response of shallow layers probably accounts for this discrepancy, an inference supported by the strong site effects observed in the Annecy Basin, which amplified ground motion by a factor of up to 8 at resonant frequencies.

The main observation still needing an explanation is possibly why aftershocks only occurred in the sedimentary cover while the Vuache Fault is considered, on geological grounds, to extend into the Variscan basement. The idea of a cover fault stretching for tens of kilometres without cutting into the basement is consistent with a decollement-and-lateral-ramp tectonic style, consistent with thin-skinned overthrusting in the Jura Mountains and Subalpine chains (e.g. Guellec et al. 1990), but not with basement reactivation.

If one takes extreme error bounds, the main shock could have occurred in the upper part of the basement (e.g. at 4 km depth), where it might have triggered only a few very small, undetected aftershocks, while fracture within the sedimentary cover was more extensive. If this had been the case, the aftershocks we located would not image the rupture plane of the Epagny earthquake. We find this inference unlikely. What makes this explanation even more difficult to defend is that aftershocks of strike-slip earthquakes are commonly restricted to the rupture plane (e.g. Scholz 1990).

Alternatively, the Vuache Fault might root deep into the basement but exhibit a kink at the cover–basement interface, which would have stopped rupture there and might decouple larger deep events from smaller shallow ones. There is no evidence for this kink, neither in the present seismological data nor in seismic exploration sections. Therefore, we definitely consider the Vuache Fault to be a cover feature. However, the kink hypothesis must be tested thoroughly, because it might hold the key to the occurrence of rare M6 events on the longer, most quiescent segments of the Vuache Fault.

ACKNOWLEDGMENTS

This study was supported by the Institut National des Sciences de l'Univers, Paris. It benefited from the availability of data from several networks [Sismalp (Grenoble), LDG/CEA (Bruyeres-le-Chatel), SED (Zurich), IGG (Genova), and ReNaSS (Strasbourg)]. P. Hoang-Trong (Bureau Central Seismologique Français) kindly provided data for drawing isoseismal curves. The strong-motion data for the site-effect study was acquired by the Reseau Accelerometrique Mobile. R. Guiguet, M. Lambert and G. Poupinet also helped in collecting aftershock data. We thank J. Riepl for providing us with her general inversion program. Most figures were drawn using the GMT library (Wessel & Smith 1991). N. Deichmann pointed out small inconsistencies in the first version of this paper; G. Bock improved it through constructive remarks. We are grateful to both of them.

REFERENCES

Aki, K. & Richards, P.G., 1980. Quantitative Seismology. Theory and Methods, Vol. 1, Freeman, San Francisco.

Amato, E., 1983. Etude de la seismicite historique de la faille du Vuache (Haute-Savoie, France), Dipl., University of Geneve.

Arikan, Y., 1964. Etude geologique de la chaine Grand Credo-Vuache (Ain, Haute-Savoie), These, University of Geneve.

Billiet, A., 1851. Memoire sur les tremblements de terre ressentis en Savoie, Mem. Acad. R. Savoie, **1,** 245–288.

Blondel, T., Charollais, J., Sambeth, U. & Pavoni, N., 1988. La faille du Vuache (Jura meridional): un exemple de faille a caractere polyphase, Bull. Soc. vaud. Sci. Nat., **79,** 65–91.

Bock, G., 1997. GeoForschungsZentrum (GFZ), in A Rapid Warning System for Earthquakes in the European-Mediterranean Region, 1st Yr Progr. Rep., Europ. Comm., DG XII, 54–60.

Charollais, J., Clavel, B., Amato, E., Escher, A., Busnardo, R., Steinhauser, N., Macsotay, O. & Donse, P., 1983. Etude preliminaire de la faille du Vuache (Jura meridional), Bull. Soc. vaud. Sci. Nat., **76,** 217–256.

Chauve, P., Enay, R., Fluck, P. & Sittler, C., 1980, Vosges-Fosse rhenan-Bresse-Jura, Ann. sci. University Besançon, Geol., **4**.

Cornou, C., 1997. Etude des premieres donnees du Reseau accelerometrique permanent, DEA Phys. Chim. Terre, Univ. L.-Pasteur, Strasbourg.

Correspondenzblatt des koniglich Wurttembergischen landwirthschaftlichen Vereins, 1840. **27**.

Dufumier, H. & Rouland, D., 1998. Moment tensor inversions for some recent earthquakes in France, XXVI Gen. Ass. European Seism. Comm., Tel Aviv, Aug. 23–28.

Field, E.H. & Jacob, K.H., 1993. A comparison and test of various site-response estimation techniques, including three that are not reference-site dependent, Bull. seism. Soc. Am., **85,** 1127–1143.

Frechet, J., 1978. Sismicite du Sud-Est de la France, et une nouvelle methode de zonage sismique, These 3e cycle, Univ. Sci. Med., Grenoble.

Frechet, J., Thouvenot, F., Jenatton, L., Hoang-Trong, P. & Frogneux, M., 1996. Le seisme du Grand-Bornand (Haute-Savoie) du 14 decembre 1994: un coulissage dextre dans le socle subalpin, C. R. Acad. Sci. Paris, **323,** 517–524.

Gaudemer, Y., Tapponnier, P., Meyer, R., Peltzer, G., Shunmin, G., Zhitai, C., Huagung, D. & Cifuentes, I., 1995. Partitioning of crustal slip between linked, active faults in the eastern Qilian Shan, and evidence for a major seismic gap, the 'Tianshu gap', on the western Haiyuan Fault, Gansu (China), Geophys. J. Int., **120,** 599–645.

Guellec, S., Mugnier, J.-L., Tardy, M. & Roure, F., 1990. Neogene evolution of the western Alpine foreland in the light of ECORS data and balanced cross-sections, in Deep Structure of the Alps, eds Roure, F., Heitzmann, P. & Polino, R., Mem. Soc. geol. Fr., **156,** 165–184.

Jalil, W. & Bisch, P., 1997. Les effets sur les batiments: aspects structuraux, in Le seisme d'Epagny (Haute-Savoie, France) du 15 juillet 1996, Rapport de mission, AFPS, Paris.

Journal de Geneve, 1839. 31 August 1839.

Journal de Savoie, 1839. 24 August 1839.

Kagan, Y.Y. & Jackson, D.D., 1995. New seismic gap hypothesis: five years after, J. geophys. Res., **100,** 3943–3959.

Kanamori, H., 1977. The energy release in great earthquakes, J. geophys. Res., **82,** 2981–2987.

Lambert, J. & Levret-Albaret, A., eds, 1996. Mille ans de seismes en France. Catalogue d'epicentres. Parametres et references, Ouest Edns, Nantes.

Le Brun, B., 1997. Les effets de site: etude experimentale et simulation de trois configurations, These, Univ. J.-Fourier, Grenoble.

Lee, W.H.K. & Lahr, J.C., 1975. HYPO71 (revised.): a computer program for determining hypocenter magnitude, and first motion pattern of local earthquakes, USGS Open File Rept, **75–311**.

Massinon, B., 1979. Vue d'ensemble de la sismicite instrumentale en France de 1962 a 1976, in Les tremblements de terre en France, ed. Vogt, J., Mem. Bur. Rech. geol. Min., **96,** 193–202.

Menard, G., 1988. Structure et cinematique d'une chaine de collision— Les Alpes occidentales et centrales, These d'Etat, Univ. Sci. Med., Grenoble.

Nicolas, M., Santoire, J.-P. & Delpech, P.-Y., 1990. Intraplate seismicity: new seismotectonic data in western Europe, Tectonophysics, **179,** 27–53.

Omori, F., 1907. Strong earthquakes in the Shinanogawa drainage area in recent years, Tokyo Gakugei Zasshi, **24,** 114–117 (in Japanese).

Reasenberg, P. & Oppenheimer, D., 1985. FPFIT, FPPLOT and FPPAGE: Fortran computer programs for calculating and displaying earthquake fault-plane solutions, USGS Open File Rept, **85–739**.

Riepl, J., Bard, P.-Y., Hatzfeld, D., Papaioannou, C. & Nechtschein, S., 1998. Detailed evaluation of site-response estimation methods across and along the sedimentary valley of Volvi (EURO-SEISTEST), Bull. seism. Soc. Am., **88,** 488–502.

Rigassi, D., 1977. Encore le Risoux, Bull. Soc. vaud. Sci. Nat., **73,** 379–413.

Rothe, J.-P., 1941. La seismicite des Alpes occidentales, Ann. Inst. Phys. Globe Strasbourg, **3,** 26–100.

Rothe, J.-P., 1972. La seismicite de la France de 1961 a 1970, Ann. Inst. Phys. Globe Strasbourg, **9,** 3–134.

Sambeth, U., 1984. Seismotektonische Untersuchungen im Gebiet des Genfer Beckens, Dipl., ETH Zurich.

Sambeth, U. & Pavoni, N., 1988. A seismotectonic investigation in the Geneva Basin, southern Jura mountains, Eclogae geol. Helv., **81,** 433–440.

Schardt, H., 1891. Etudes geologiques sur l'extremite meridionale de la premiere chaine du Jura (Chaine du Reculet-Vuache), Bull. Soc. vaud. Sci. Nat., **27,** 69–158.

Scholz, C.H., 1990. The Mechanics of Earthquakes and Faulting, Cambridge University Press, Cambridge.

Sellami, F., Kissling, E., Thouvenot, F. & Frechet, J., 1995. Initial reference velocity model for seismic tomography in the western Alps, 20th Gen. Ass. EGS., Hamburg.

Serand, J., 1909. Liste chronologique des tremblements de terre observes dans le departement de la Haute-Savoie, Rev. Savoisienne, **50,** 327–332.

Solarino, S., Kissling, E., Sellami, S., Smriglio, G., Thouvenot, F., Granet, M., Bonjer, K.P. & Sleijko, D., 1997. Compilation of a recent seismicity data base of the greater Alpine region from several seismological networks and preliminary 3D tomographic results, Ann. Geofis., **XL,** 161–174.

Thouvenot, F., 1996. Aspects geophysiques et structuraux des Alpes occidentales et de trois autres orogenes (Atlas, Pyrenees, Oural), These d'Etat, Univ. J.-Fourier, Grenoble.

Vogt, J., ed., 1979. Les tremblements de terre en France, Mem. Bur. Rech. Geol. Min., **96**.

Wessel, P. & Smith, W.H.F., 1991. Free software helps map and display data, EOS, Trans. Am. geophys. Un., **72,** 441; 445–446.